The University of Texas ARLINGTON

MATHEMATICS
Preprint Series

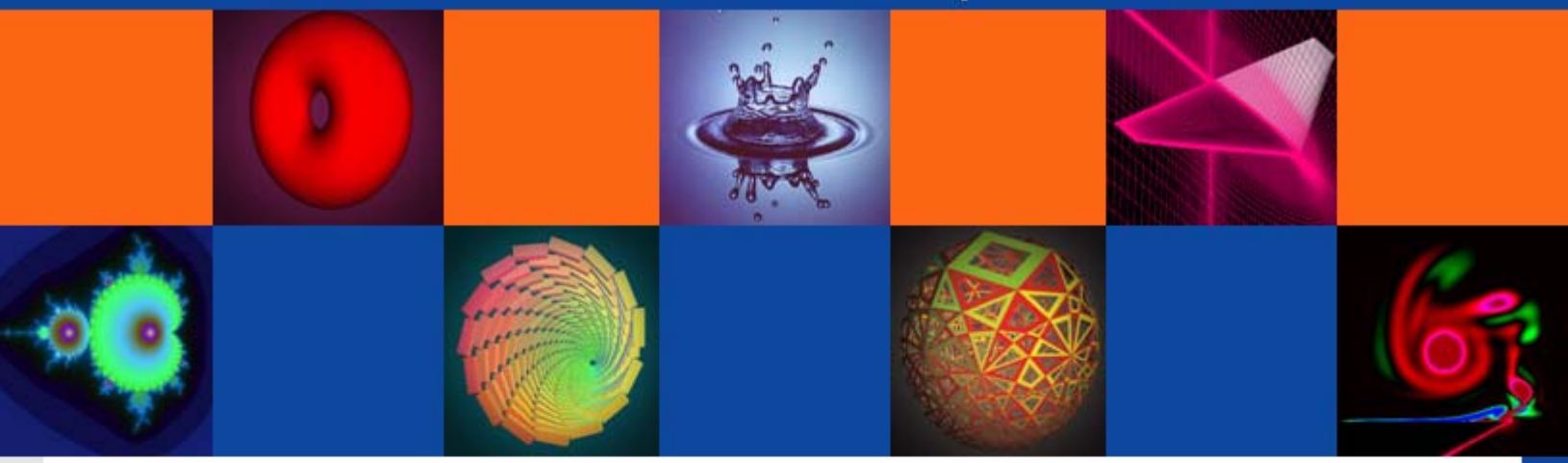

A Three-dimensional Bay/Estuary Model for Hydrodynamics and Salinity Transport

H. Shan, G.T. Yeh, G. Hu, T.S. Wu

Technical report 2007-04

http://www.uta.edu/math/preprint/

A Three-dimensional Bay/Estuary Model for Hydrodynamics and Salinity Transport

Hua Shan [a, *], Gour-Tsyh Yeh [b], Gordon Hu [c], Tien-Shuenn Wu [d]

[a] Department of Mathematics, University of Texas at Arlington, Arlington, TX 76019
[b] Department of Civil and Environmental Engineering, University of Central Florida, Orlando, FL 32816
[c] South Florida Water Management District, 3301 Gun Club Road, [c] West Palm Beach, FL 33406
[d] Florida Department of Environmental Protection, 2600 Blair Stone Road, [d] MS 3555, Tallahassee, FL 32399

Abstract

This paper presents the development and application of a bay/estuary model to simulate hydrodynamics and salinity transport. The hydrodynamic module solves three-dimensional Navier-Stokes equations with or without the hydrostatic assumptions. The Boussinesq approximation is employed to deal with the buoyancy force due to temperature and salinity variations. The moving free surface is explicitly handled by solving the kinematic boundary condition equation using a node-repositioning algorithm. The transport module solves the mass transport equation for the salinity field. The Arbitrary Lagrangian-Eulerian (ALE) representation is adopted for all transport equations including momentum transport. The solution is obtained with the finite element method or the mixed Lagrangian-Eulerian (particle tracking) and finite element method. The model has been successfully calibrated with tides and salinities and is applied to Loxahatchee Estuary for the investigation of its minimum flow requirements to maintain ecological balance.

Keywords: hydrodynamics model, free surface, salinity transport, numerical simulation.

* Corresponding author. Email: hshan@uta.edu

1. Introduction

The modeling and numerical simulation of flow and transport in bay and estuary are very important for coast engineering, environmental protection, and disaster planning. In the past, the numerical models based on the hydrostatic assumption and the depth-integrated shallow water equations are widely used (Duwe et al., 1983; Le Provost et al., 1995; Benque et al., 1998; Sauvaget et al., 2000). Over the past few years, there has been growing demanding of three-dimensional hydrodynamics models in estuarine studies. However, the majority of these models are based on the multi-layer or the multi-level approaches (Drago et al. 2000; Kim et al. 1994; Shankar et al. 1997; and Zhang & Gin 2000). In the multi-layer approach, the column of water is divided into layers that can move freely in the vertical direction to maintain continuity, but there is no transport across layers. Furthermore, the application of multi-layer model to simulate tidal currents requires the strict specification of open boundary conditions at the layer interfaces, which is rather difficult to obtain in practical situations. The multi-level model, on the other hand, describes the vertical motion of fluid in terms of vertical transport between the various levels, while the interfaces between the layers are fixed in space. Compared to fully three-dimensional models, multi-level modeling is not convenient in areas where high vertical gradient of density are present. As a matter of fact, both multi-layer model and multi-level model are composed of a stacking of many depth-averaged hydrodynamic models in the vertical direction. Within each layer, the hydrostatic assumption and the depth-integration are still required. Sometimes a fully three-dimensional hydrodynamic model based on the Navier-Stokes equations is needed in order to provide reliable description of convective dynamics. As it is commonly believed that the Navier-Stokes equations are the general governing equations for fluid flows, a model rooted in the Navier-Stokes equations is valid for flow motions over a large range of length-scales.

Generally fluid flows can be described using one of the following three approaches, i.e. the Lagrangian representation, the Eulerian representation, and the arbitrary Lagrangian-Eulerian (ALE) representation. In the Lagrangian representation, the governing equations are expressed in the form of material derivatives, and therefore the

convection terms vanish in the equations. The Eulerian representation is widely used for flow problems in a fixed domain. The non-linear convection terms in the governing equations require some special techniques, such as the upwind scheme, if the flow is dominated by convection. The ALE method introduced by Chan (1975) is a general representation between Lagrangian and Eulerian approaches. As indicated by Braess and Wriggers (2000), the ALE representation can be converted to Lagrangian or Eulerian representation.

In the modeling of flow and transport in bay and estuary, the fluid is not contained in a fixed domain. The evaluation of the unsteady free surface becomes part of the solution, thus an accurate description of the geometry of the free surface and its evolution in time becomes critical. From the point of view of computational method, two approaches are available, namely the fixed-grid approach and the moving grid approach.

In the fixed-grid approach, the grid used to solve the flow problem is entirely or quasi-entirely fixed and the equations are expressed using the Eulerian representation. Since the grid is fixed, the free surface may be treated with one of the following three methods. The first one is commonly known as the marker method, such as the marker and cell (MAC) method proposed by Harlow and Welch (1965). In this method, massless tracers or marker particles are used in the algorithm to determine the position of the surface. Interfacial or surface-marker methods use marker particles only on the interfaces. Volume-marker methods have marker particles in the whole domain. The free surface is reconstructed by following the massless interface particles that move with the flow at local fluid velocity. Usually the MAC method requires large memory size to store and track markers distributed in the fluid region. The second method is the volume of fluid (VOF) method introduced by Hirt and Nichols (1981). This algorithm incorporates a transport equation for a void function, which is used to identify the free surface. VOF is very efficient in simulating the transient fluid flow with a free surface. However, it has drawbacks in that the position of the free surface is predicted only by the scalar fractional volume value and the filling state of the neighbor cells. Thus, in order to predict the geometry of the free surface accurately, the size of the cell must be sufficiently small near

the free surface. The third method is the implement of hydrostatic assumption commonly used in modeling tidal circulations. In this method, the free surface is determined from a vertically integrated continuity equation. The Navier-Stokes equation is then reduced to two horizontal equations, the vertically integrated continuity equation, the original continuity equation, and the hydrostatic equation that replaces the vertical momentum equation. The first four equations are solved for the free-surface elevation and three velocity components. The fifth equation is then used to calculate the pressure distribution. Although this method may allow good predictions in free-surface elevation, it may not predict the vertical circulation and thus the horizontal circulation accurately, since the vertical momentum equation is reduced to the hydrostatic assumption.

A moving grid method can be used to track the deformation of the free surface. The moving grid method is usually combined with the Lagrangian representation or the ALE representation of the governing equations. In the Lagrangian representation, the governing equations are expressed in the form of material derivatives, and therefore the convection terms vanish in the equations. In this case, the grid in the deformed domain should strictly follow the local velocity of the fluid and thus may result in severe skew in domain mesh, especially for complex flow conditions involving circulations and vortices. When the ALE representation is used, arbitrary velocity can be assigned to grid node and the grid movement in the interior of the domain becomes independent of the velocity field. On the free surface, it is not necessary for the grid node to follow the local velocity as far as the movement of the grid node reflects the deformation of the surface. It is possible for the ALE method to maintain reasonably shaped meshes and describe the free surface boundary accurately at the same time.

In this paper we present a three-dimensional bay/estuary surface water model to simulate hydrodynamics and salinity transport. The temperature transport is also included in the model but not in this paper. This surface water model has two basic components: the hydrodynamic module and the transport module. The hydrodynamic module is based on the three-dimensional Navier-Stokes equations with or without the hydrostatic assumptions. The transport module solves the transport equation of thermal energy and

the transport equations of salinity as well as transport equations of turbulent energy and generic turbulent parameter. A moving grid method based on node-repositioning is used to track the deformation of water surface. The ALE representation is adopted for all transport equations. The surface water domain is discretized using finite element mesh, which is more flexible in modeling bay/estuary with complex geometry. The numerical solution is obtained using the finite element method or the mixed Lagrangian-Eulerian (particle tracking) and finite element method (Cheng, et al., 1996). The proposed model has been successfully calibrated with tides and salinities and is applied to Loxahatchee River and Estuary in Florida.

This paper is arranged as follows: Section 2 describes mathematical model including the governing equations and the boundary conditions. Section 3 reveals some details of the numerical methods including the temporal and spatial discretization, the particle tracking algorithm, and the moving grid scheme. A preliminary verification of the model is presented in Section 4. The application of the model to the Loxahatchee River is presented in Section 5. The concluding remarks can be found in Section 6.

2. Mathematical model

2.1 Governing equations

In modeling the flow problem with free surface, the moving grid method is used in combination with the Arbitrary Lagrangian-Eulerian (ALE) representation (Chan, 1975) of the governing equations. The moving grid approach allows the mesh to move to accommodate the deformation of the free surface and the movement of the mesh node does not necessarily follow the motion of fluid particle. Namely the mesh can move arbitrarily to fit the free surface. The ALE representation can be converted to Lagrangian or Eulerian representations (Braess & Wriggers, 2000). The ALE representation adopts a notation "$d\Psi/dt$" for the total derivative of Ψ. The Eulerian derivative denoted by "$\partial\Psi/\partial t$" is related to the total derivative in the form of

$$\frac{d\Psi}{dt} = \frac{\partial\Psi}{\partial t} + \mathbf{V}_g \cdot \nabla\Psi \tag{1}$$

where $\mathbf{V}_g$ is the grid moving velocity. The Lagrangian derivative of Ψ can be written as

$$\frac{D\Psi}{Dt} = \frac{\partial \Psi}{\partial t} + \mathbf{V} \cdot \nabla \Psi \tag{2}$$

where $\mathbf{V}$ is the vector of flow velocity. Using Equations (1) and (2), the relationship between the ALE total derivative and the Lagrangian derivative is found as

$$\frac{D\Psi}{Dt} = \frac{d\Psi}{dt} + (\mathbf{V} - \mathbf{V}_g) \cdot \nabla \Psi$$

In the surface water domain, the governing equations are the three-dimensional Navier-Stokes equations for incompressible flow including the continuity equation and momentum equation. The continuity equation that states the conservation of mass is given by

$$\nabla \cdot \mathbf{V} = Q \tag{3}$$

where Q is the mass source/sink term. The momentum equation in the ALE form is written as

$$\begin{aligned} &\frac{d\mathbf{V}}{dt} + (\mathbf{V} - \mathbf{V}_g) \cdot \nabla \mathbf{V} + (\nabla \cdot \mathbf{V})\mathbf{V} = \\ &- \nabla \Phi - \frac{\Delta \rho}{\rho_0} g \nabla z + \frac{1}{\rho_0} \nabla \cdot \boldsymbol{\tau} - 2\boldsymbol{\Omega} \times \mathbf{V} + Q\mathbf{V}_* \end{aligned} \tag{4}$$

where $\Phi = p/\rho_0 + gz$ is the potential, p is the pressure, ρ_0 is the reference density of water, g is the gravitational acceleration, $2\boldsymbol{\Omega} \times \mathbf{V}$ is the Coriollis force, and $\mathbf{V}_*$ is the velocity of source flow. The Boussinesq approximation is employed to deal with the buoyancy force reflected by $\Delta\rho$ which is the change of density due to temperature and salinity. $\boldsymbol{\tau}$ is the turbulence stress tensor and is modeled using the generic length scale (GLS) turbulence model (Umlauf et al., 2003; and Warner et al., 2005), which is the generalized formulation of many two-equation closures turbulence models. It solves the standard transport equation for turbulent kinetic energy and another transport equation for a generic parameter. Interested reader should refer to Umlauf et al.(2003) and Warner et al.(2005) for more details.

The time evolution of the free water surface elevation is governed by the following equation

$$\frac{d\eta}{dt} + (u_s - u_g)\frac{\partial \eta}{\partial x} + (v_s - v_g)\frac{\partial \eta}{\partial y} = w_s + R - E \tag{5}$$

where η is the free surface elevation with respect to a reference elevation H_0 as shown in Figure 1. $u_s, v_s,$ and w_s are the three components of flow velocity on the free surface. u_g and v_g are the horizontal components of the moving grid velocity on the free surface. R and E represent the rainfall and evaporation intensity, respectively. Equation (5) also represents a kinematic boundary condition, which states the fact that the free surface is a material surface, i.e., the fluid particles initially locate on the free surface always remain on the surface.

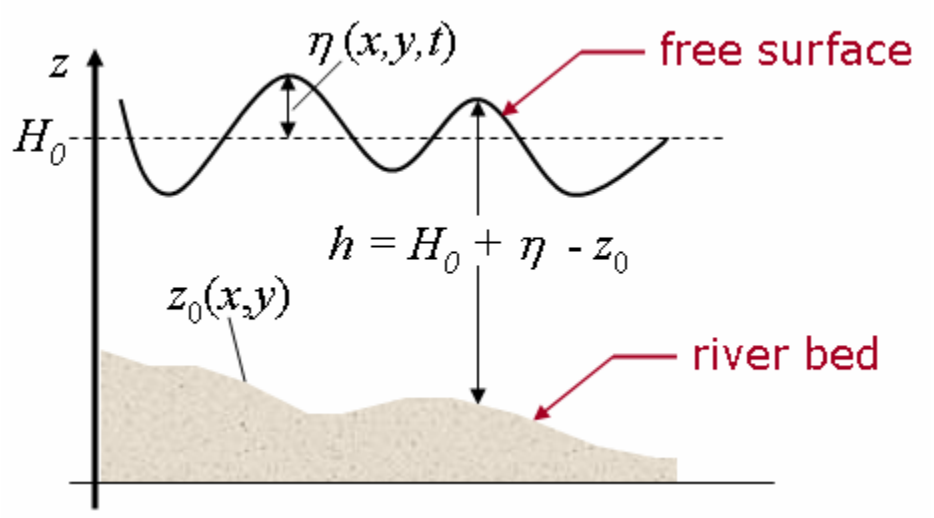

Figure 1 Schematic sketch of free surface and notations

Equations (1), (2), and (3) represent a fully hydrodynamic model. In some applications where the horizontal length scale is much larger than the vertical length scale, the vertical component of acceleration has a negligible effect on the pressure, thus the hydrostatic assumptions applies to the pressure. Under the hydrostatic assumption, the governing equations in the Lagrangian form can be written as

$$\frac{D_H h}{Dt} = -(\nabla_H \cdot \bar{\mathbf{V}})h + \bar{Q}h + R - E - I \tag{6}$$

$$\frac{D\,u}{D\,t} + (\nabla \cdot \mathbf{V})\,u = - \frac{\partial\,\Phi}{\partial\,x} + \frac{1}{\rho}[\frac{\partial}{\partial\,x}(\tau_{xx}) + \frac{\partial}{\partial\,y}(\tau_{yx}) + \frac{\partial}{\partial\,z}(\tau_{zx})] - 2(\Omega_y w - \Omega_z v) + Q u_* \tag{7}$$

$$\frac{D\,v}{D\,t} + (\nabla \cdot \mathbf{V})\,v = - \frac{\partial\,\Phi}{\partial\,y} + \frac{1}{\rho}[\frac{\partial}{\partial\,x}(\tau_{xy}) + \frac{\partial}{\partial\,y}(\tau_{yy}) + \frac{\partial}{\partial\,z}(\tau_{zy})] - 2(\Omega_z u - \Omega_x w) + Q v_* \tag{8}$$

$$\frac{\partial}{\partial\,z}(\frac{p}{\rho_0} + g\,z) + \frac{\Delta\,\rho}{\rho_0} g = 0 \tag{9}$$

where h in Equation (6) is the water depth, and $h = \eta + H_0 - z_0$ (see Figure 1). I is the infiltration intensity. $\bar{Q}$ is the depth-averaged mass source/sink. $\bar{\mathbf{V}} = \{\bar{u}, \bar{v}\}^{\mathrm{T}}$ is the vector of depth-averaged velocity, and $\bar{u}$ and $\bar{v}$ are the x- and y-component of the depth-averaged velocity. $\nabla_H \cdot \bar{\mathbf{V}}$ is the divergence of depth-averaged velocity and is defined as $\nabla_H \cdot \bar{\mathbf{V}} = (\partial\bar{u}/\partial x) + (\partial\bar{v}/\partial y)$. In Equation (6), the Lagrangian derivative of water depth ($D_H h/Dt$) associated with the depth-averaged velocity can be defined as $D_H h/Dt = \partial h/\partial t + \bar{u}(\partial h/\partial x) + \bar{v}(\partial h/\partial y)$. Equations (7) and (8) are the x- and y-momentum equations. Under the hydrostatic assumption, the z- momentum equation is reduced to Equation (9).

The governing equation for salinity transport is written in the ALE form as

$$\frac{d\,S}{d\,t} + (\mathbf{V} - \mathbf{V}_g) \cdot \nabla S + (\nabla \cdot \mathbf{V})\,S = \nabla \cdot (K_S \nabla S) + Q S_* \tag{10}$$

where S is the salinity, K_S is the saline dispersion/diffusion coefficient, and S_* is the salinity of source. Anisotropy in the saline dispersion/diffusion coefficient can be easily incorporated by replacing K_S with a second-order tensor. Equation (10) can also be written in the Lagrangian form as

$$\frac{D S}{D t} + (\nabla \cdot \mathbf{V}) S = \nabla \cdot (K_S \nabla S) + Q S_* \tag{11}$$

2.2 Boundary conditions for flow

A wide range of various types of boundary conditions for the Navier-Stokes equations are incorporated in order to deal with as wide range of realistic problems as possible. Five different types of boundary conditions are summarized below.

1. Dirichlet Boundary Condition: On a Dirichlet boundary, the state variables of flow are prescribed. The general form of the Dirichlet boundary condition is given by

$$\boldsymbol{\Psi}\Big|_{\Gamma_D} = \boldsymbol{\Psi}_D \tag{12}$$

where $\boldsymbol{\Psi} = \{\Phi, u, v, w, \eta \,(\text{or } h)\}^{\mathrm{T}}$. $\boldsymbol{\Psi}_D$ represents prescribed value of $\boldsymbol{\Psi}$ on the Dirichlet boundary Γ_D.

2. Free Surface Boundary Condition: On the free surface, the conservation of momentum leads to the following dynamic boundary condition, if the surface tension is negligible.

$$\mathbf{n} \cdot \boldsymbol{\sigma} = \mathbf{n} \cdot \boldsymbol{\sigma}_{ext} \tag{13}$$

where $\mathbf{n}$ is the outward-pointing unit vector normal to the free surface. $\boldsymbol{\sigma}$ is the total stress tensor of the internal fluid in the computational domain, e.g. the stress tensor of water in the surface water model. $\boldsymbol{\sigma}_{ext}$ is stress tensor of the external fluid, such as air. If the pressures on both sides of the interface are assumed equal, and the external stress only includes wind stress, then Equation (13) becomes

$$\mathbf{n} \cdot \boldsymbol{\tau} = \mathbf{n} \cdot \boldsymbol{\tau}_{wind} \tag{14}$$

where $\boldsymbol{\tau}_{wind}$ is the wind stress at the free surface.

3. River-Bed Boundary Condition: On the river bed, the continuity of normal stress leads to a boundary condition similar to Equation (14).

$$\mathbf{n}\cdot\boldsymbol{\tau} = \mathbf{n}\cdot\boldsymbol{\tau}_{bed} \tag{15}$$

where $\mathbf{n}$ is the outward-pointing unit vector normal to the river bed, and $\boldsymbol{\tau}_{bed}$ is the river bed stress.

4. Moving Contact Wall Condition: The moving contact surface is the interface between the fluid and solid wall on which the free surface may slide up and down as water elevation rises and falls. To allow the free surface slide along the contact surface, one cannot impose the no-slip boundary condition. Therefore, either the perfect slip boundary condition

$$\mathbf{n}\cdot\mathbf{V}\Big|_{\Gamma_M} = 0 \tag{16}$$

or the Navier's condition (Güler et al., 1999)

$$[(\mathbf{I}-\mathbf{n}\,\mathbf{n})\cdot(\mathbf{n}\cdot\boldsymbol{\tau}) + \frac{1}{\sigma}(\mathbf{I}-\mathbf{n}\,\mathbf{n})\cdot\mathbf{V}]\Big|_{\Gamma_M} = 0 \tag{17}$$

is specified on moving contact surfaces. $\mathbf{n}$ is the outward-pointing unit vector normal to the moving contact surface, σ is an empirical slip coefficient, and Γ_M indicates the moving contact boundary.

5. Radiation Boundary Condition: The following radiation boundary condition is used along the open-sea boundaries of the computational domain

$$\eta - \frac{\mathbf{n}\cdot\mathbf{V}\,h}{\sqrt{g\,h}}\Bigg|_{\Gamma_R} = 2\eta_R \tag{18}$$

where η is the free surface elevation relative to the sea-level datum, $\mathbf{n}$ is the outward-pointing unit normal vector of the boundary, $\mathbf{V}$ is the flow velocity vector, h is the water depth, η_R is the equivalent progressive wave amplitude, and Γ_R indicates the radiation boundary. Along the open-sea boundaries, the water surface elevation is composed of periodic tidal components and a transient or low frequency component of the sub-tidal

frequency spectrum. The equivalent progressive wave amplitude in Equation (18) is given by

$$\eta_R = \eta_{LF} + \sum_{m=1}^{M} \left(\eta_{RCm} \cos(\omega_m t) + \eta_{RSm} \sin(\omega_m t) \right)$$

where η_{LF} is the water surface elevation corresponding to low frequency component, M is the number of tidal constituents, ω_m is the wave number of the m-th frequency. η_{RCm} and η_{RSm} are amplitudes of the sinusoidal waves.

2.3 Boundary conditions for salinity transport

This model incorporates a wide range of boundary conditions for salinity transport. Specifically, the following five types of boundary conditions can be specified at the global boundary.

1. Dirichlet Boundary Condition: On Diriclet boundaries, the salinity is prescribed. The Dirichlet boundary condition for salinity is given by

$$S\big|_{\Gamma_D} = S_D \tag{19}$$

where Γ_D indicates the boundary where the Dirichlet boundary condition is specified, and S_D is the prescribed value of S on the boundary.

2. Neumann Boundary Condition: On the Neumann boundary, the gradient of salinity is specified in the form of

$$-\mathbf{n} \cdot (K_S \nabla S)\big|_{\Gamma_N} = q_N \tag{20}$$

where **n** is the outward-pointing unit normal vector of the boundary, Γ_N indicates the boundary where the Neumann boundary condition is specified, and q_N is the prescribed flux due to diffusion on the boundary.

3. Cauchy Boundary Condition: On the Cauchy boundaries, the total flux of salinity is prescribed. The Cauchy boundary condition for salinity can be written as

$$\mathbf{n}\cdot(\mathbf{V}\,S)-\mathbf{n}\cdot(K_S\nabla S)\Big|_{\Gamma_C}=q_C \tag{21}$$

where Γ_C indicates the boundary where the Cauchy boundary condition is specified and q_C is the prescribed flux due to convection and diffusion on the boundary.

4. Variable Boundary Condition: On the variable boundaries, either the incoming salinity is prescribed or the salt is carried out by advection. The general form of the variable boundary condition for any scalar transport is given by the variable boundary condition for salinity can be written as

$$\begin{cases} -\mathbf{n}\cdot(K_S\nabla S)\Big|_{\Gamma_V}=0 & \text{if } \mathbf{n}\cdot\mathbf{V}\geq 0 \\ \mathbf{n}\cdot(\mathbf{V}\,S)-\mathbf{n}\cdot(K_S\nabla S)\Big|_{\Gamma_V}=q_V & \text{if } \mathbf{n}\cdot\mathbf{V}<0 \end{cases} \tag{22}$$

where q_V is inflow flux, and Γ_V represents the boundary where a variable boundary condition is imposed. On the variable boundary, under the outflow condition ($\mathbf{n}\cdot\mathbf{V}\geq 0$), the flux due to diffusion is set to zero; under the inflow condition ($\mathbf{n}\cdot\mathbf{V}<0$), the total inflow flux is given by q_V.

5. Flushing Boundary Condition: On the open-ocean boundaries, the salinity is carried out of the region of interest by currents during ebb tides. During flood tides, the salinity returns to the region of interest from the open sea with decay due to flushing characteristics of the estuary. This type of boundary conditions is mathematically described as

$$\begin{cases} -\mathbf{n}\cdot(K_S\nabla S)\Big|_{\Gamma_F}=0 & \text{if } \mathbf{n}\cdot\mathbf{V}\geq 0 \\ S\Big|_{\Gamma_F}=S_0-(S_0-S_{et})\,e^{-\lambda_S(t-t_{et})} & \text{if } \mathbf{n}\cdot\mathbf{V}<0 \end{cases} \tag{23}$$

where Γ_V represents the boundary where a variable boundary condition is imposed, S_0 is the value of S in the ocean far away from the boundary; S_{et} is the value of S at the end of the last ebb tide on the boundary, t_{et} is the time corresponding to the end of the last

ebb tide on the boundary, and λ_S is the damping coefficient. Under the outflow condition ($\mathbf{n}\cdot\mathbf{V}\geq 0$), the flux due to diffusion is set to zero; under the inflow condition ($\mathbf{n}\cdot\mathbf{V}<0$), the salinity on the boundary is set to $S_0(1-e^{-\lambda_S(t-t_{et})})+S_{et}e^{-\lambda_S(t-t_{et})}$.

3. Numerical methods

3.1 Finite element method

The governing equations (3)-(5) for the non-hydrostatic model with boundary conditions (12)-(18) and the salinity transport equation given by (10) with boundary conditions (19)-(23) can be solved using the finite element method. The commonly adopted standard Galerkin finite element method (GFEM) exhibits global spurious oscillations when the flow is dominated by convection. To avoid the numerical oscillation, a Petrov-Galerkin finite element method (PGFEM) known as the Streamline Upwind Petrov-Galerkin (SUPG) method (Brooks, et al., 1982) is utilized. More details have been presented elsewhere (Shan and Yeh, 2004).

3.2 Mixed Lagrangian-Eulerian and finite element method

The governing equations (6)-(9) for the hydrostatic model with boundary conditions (12)-(18) and the salinity transport equation given by (11) with boundary conditions (19)-(23) can be solved using the mixed Lagrangian-Eulerian (particle tracking) and finite element methods. We take the salinity transport equation as an example. Equation (11) can be discretized in time as

$$\frac{S^{n+1}-S^{*}}{\Delta\tau} = \frac{1}{2}[\nabla\cdot(K_S\nabla S) + Q(S_*-S)]^{n+1}+\frac{1}{2}[\nabla\cdot(K_S\nabla S) + Q(S_*-S)]^{*} \qquad (24)$$

where superscript "n+1" denotes the new time step, "*" denotes the target points where the particle stops at the end of a backward tracking, and $\Delta\tau$ is elapsed travelling time of the particle. Thus, the term on the left-hand-side of Equation (24) represents an approximation to the Lagrangian derivative of salinity (DS/Dt). The details of the

backward particle tracking will be given in Subsection 3.3. Once the location of the target point is found, Equation (24) can be solved using the finite element method.

The surface water domain is partitioned with linear hexahedral, triangular-prism, or tetrahedral elements. In each element, the salinity is approximated as

$$S^h(x,y,z,t) = \sum_{\beta=1}^{N_e^l} N_\beta^l(x,y,z)\, S_\beta(t)$$

where $S^h(x,y,z,t)$ is the finite element approximation to the salinity value, $N_\beta^l(x,y,z)$ is the interpolation function of a linear element, N_e^l is number of nodes in the element, and $S_\beta(t)$ is the nodal value of salinity. The Ritz-Galerkin finite element formulation of Equation (24) in one element is written as

$$\begin{aligned}
&\frac{1}{\Delta\tau}\left(\int_{\Omega_e} W_\alpha^l N_\beta^l \, d\Omega\right) S_\beta^{n+1} + \frac{1}{2}\left(\int_{\Omega_e} \nabla W_\alpha^l \cdot (K_S \nabla N_\beta^l)\, d\Omega\right) S_\beta^{n+1} \\
&-\frac{1}{2}\left(\int_{\Gamma_e} W_\alpha^l \, \mathbf{n}\cdot(K_S \nabla N_\beta^l) d\Gamma\right) S_\beta^{n+1} + \frac{1}{2}\left(\int_{\Omega_e} W_\alpha^l Q N_\beta^l \, d\Omega\right) S_\beta^{n+1} \\
&= \frac{1}{\Delta\tau}\left(\int_{\Omega_e} W_\alpha^l S^* \, d\Omega\right) - \frac{1}{2}\left(\int_{\Omega_e} \nabla W_\alpha^l \cdot (K_S \nabla S^*)\, d\Omega\right) + \frac{1}{2}\left(\int_{\Gamma_e} W_\alpha^l \, \mathbf{n}\cdot(K_S \nabla S^*) d\Gamma\right) \\
&+\frac{1}{2}\left(\int_{\Omega_e} W_\alpha^l Q S_*^{n+1} \, d\Omega\right) + \frac{1}{2}\left(\int_{\Omega_e} W_\alpha^l Q (S_* - S)^* \, d\Omega\right) \\
&\qquad\qquad\qquad\qquad\qquad\qquad\qquad\qquad \alpha = 1, 2, \ldots, N_e^l
\end{aligned} \tag{25}$$

where W_α^l is the weighting function, Ω_e is the surface water element, and Γ_e is the boundary of the element. Equation (25) represents a local linear system for each element. Then the global linear system in a matrix form as follows is obtained through an element-by-element assembling procedure

$$\left([\mathbf{M}]+[\mathbf{B}]\right)\{\mathbf{S}\} = \{\mathbf{R}\} \tag{26}$$

where $[\mathbf{M}]$ is the mass matrix and $[\mathbf{B}]$ is the stiffness matrix. $([\mathbf{M}]+[\mathbf{B}])$ is usually a large sparse matrix and the linear system can be solved using a general sparse matrix

solver. In the application of the model to the Loxahatchee River and Estuary in Florida, the finite element mesh is generated in such a way that the grid nodes are located on the vertical lines in the z-direction, and the horizontal/vertical aspect ratio of all the elements are very large in the surface water domain. Thus, we have developed a special matrix solver based on Gauss-Seidel block iteration, and each block is formed by nodes located on the vertical line. The numerical solution procedure in one step of the nonlinear loop is shown in Figure 2.

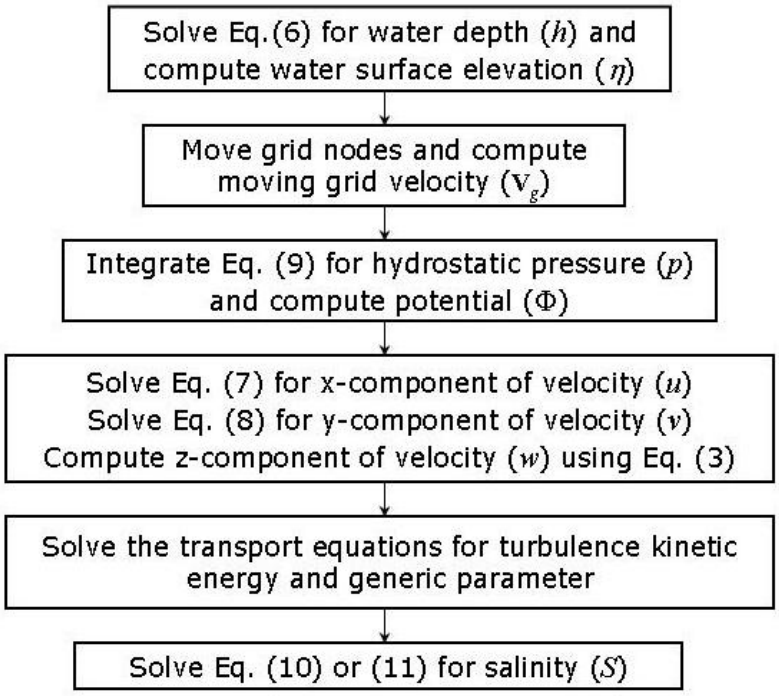

Figure 2 Solution procedure for flow and salinity transport with hydrostatic assumption

3.3 Particle tracking algorithm

In order to find the locations of the target points in the surface water domain, a backward particle tracking algorithm has been developed in the context of moving grid approach. Assume that velocity fields and locations of all grid points at current (n+1) and previous (n) time steps are known, virtual particles starting from the mesh nodes are tracked backward in time along the path line from the current time step to the previous time step. The change of velocity fields and the moving grid are taken into account by using a bilinear interpolation scheme in both space and time.

To improve the accuracy of the particle tracking, all three-dimensional global elements are further divided into sub-elements, see Figure 3 for an example, in which the hexahedral element is divided into 27 sub-elements, the triangular prism element is partitioned into 12 sub-elements, and the tetrahedral element is partitioned into 8 sub-elements. The sub-element has one of the following geometries: hexahedron, triangular prism, or tetrahedron. In one step of time marching, the backward particle tracking is divided into several sub-steps, and the particle travels within one sub-element during each sub-step. Thus the backward particle tracking algorithm is developed for the sub-element.

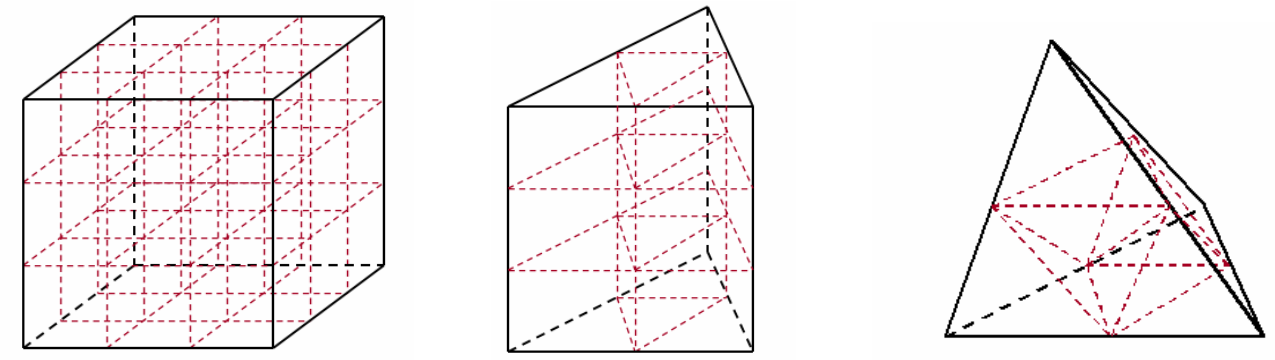

(a) hexahedral element (b) triangular prism element (c) tetrahedral element

Figure 3 Sub-elements used in backward particle tracking

In the context of moving grid method, the motion of the grid points must be taken into account. Figure 4 shows the backward particle tracking in one hexahedral sub-element. The nodes 1″ through 8″ shows the location of the sub-element at the current time step with $t = t^{n+1}$. At the previous time step with $t = t^{n}$, the location of the sub-element is denoted by nodes 1′ through 8′. Thus, the sub-element moves from the new location at $t = t^{n+1}$ to the old location at $t = t^{n}$ during one step of time marching. Also note that a deformation may occur to the element because the displacements are not necessarily the same for each node in the sub-element. A sub-step of tracking completes when the particle hits the boundary of the moving sub-element. Assume that a particle starting from a source point P at $t = t^{n+1}$ travels backward in time, the sub-step completes at $t = t^{*}$ when the particle reaches the boundary of the moving sub-element whose

location at that time is shown by nodes 1 through 8. The trajectory of the particles intersects with the boundary surface 1-2-3-4 at point Q. The boundary surface 1-2-3-4 is called the target surface and Q the target point. Apparently, the target surface is either a quadrangle or a triangle in three-dimensional particle tracking.

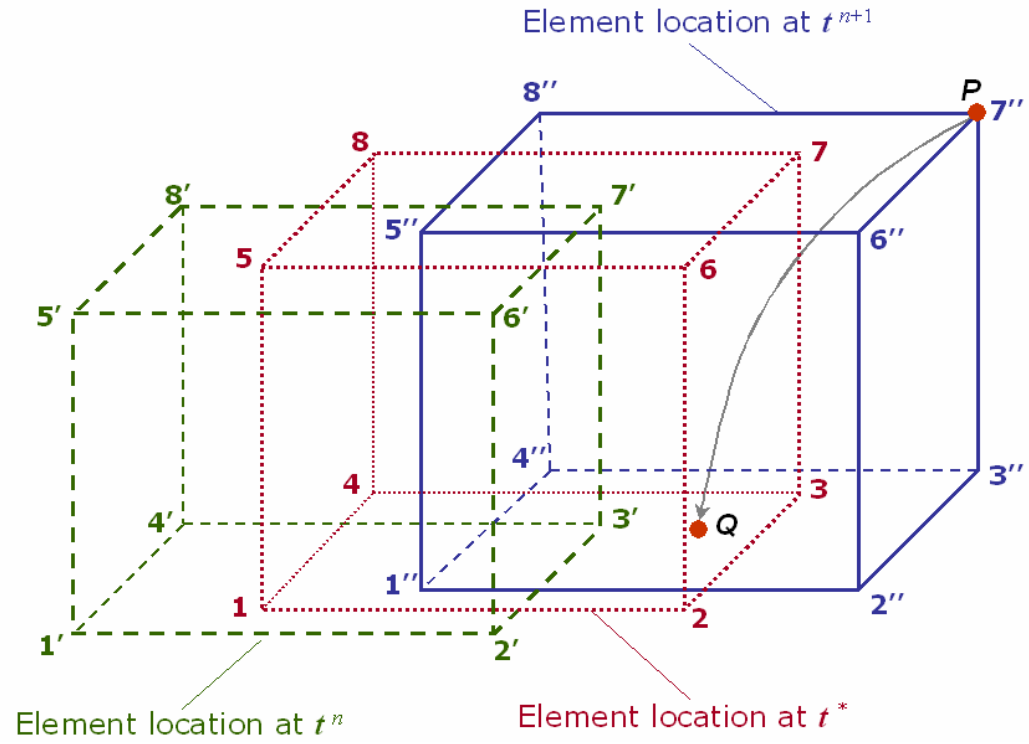

Figure 4 Backward particle tracking in a sub-element

Let $\Delta t = t^{n+1} - t^n$ be the time step size, the time fraction factor can be defined as $\theta = (t^{n+1} - t^*)/\Delta t$. If we consider the target surface of the sub-element as a two-dimensional quadrilateral or triangular element, then the coordinate (X_Q, Y_Q, Z_Q) of the target point Q can be approximated by the finite element interpolation functions as

$$X_Q = \sum_{i=1}^{N_e^{2D}} X_i N_i^l(\xi,\eta), \quad Y_Q = \sum_{i=1}^{N_e^{2D}} Y_i N_i^l(\xi,\eta), \quad Z_Q = \sum_{i=1}^{N_e^{2D}} Z_i N_i^l(\xi,\eta) \tag{27}$$

where $N_i^l(\xi,\eta)$ is the interpolation function in the local coordinate system, and N_e^{2D} is the number of nodes in the two-dimensional surface element. (X_i, Y_i, Z_i) is the nodal coordinate of the element when $t = t^*$. As indicated by Figure 4, using the time fraction factor, (X_i, Y_i, Z_i) can be calculated as

$$
\begin{aligned}
X_i &= (1-\theta) X_i^{n+1} + \theta X_i^n \\
Y_i &= (1-\theta) Y_i^{n+1} + \theta Y_i^n \qquad i = 1, \ldots, N_e^{2D} \\
Z_i &= (1-\theta) Z_i^{n+1} + \theta Z_i^n
\end{aligned} \tag{28}
$$

where $(X_i^{n+1}, Y_i^{n+1}, Z_i^{n+1})$ and (X_i^n, Y_i^n, Z_i^n) are the nodal coordinates of the surface element at time t^{n+1} and t^n, respectively. Similar to (27), the velocity of the target point can be calculated as

$$
VX_Q = \sum_{i=1}^{N_e^{2D}} VX_i N_i(\xi,\eta), \quad VY_Q = \sum_{i=1}^{N_e^{2D}} VY_i N_i(\xi,\eta), \quad VZ_Q = \sum_{i=1}^{N_e^{2D}} VZ_i N_i(\xi,\eta) \tag{29}
$$

where (VX_i, VY_i, VZ_i) is the nodal value of flow velocity in the surface element when $t = t^*$. Using the time fraction factor, (VX_i, VY_i, VZ_i) can be calculated as

$$
\begin{aligned}
VX_i &= (1-\theta) VX_i^{n+1} + \theta VX_i^n \\
VY_i &= (1-\theta) VY_i^{n+1} + \theta VY_i^n \qquad i = 1, \ldots, N_e^{2D} \\
VZ_i &= (1-\theta) VZ_i^{n+1} + \theta VZ_i^n
\end{aligned} \tag{30}
$$

where $(VX_i^{n+1}, VY_i^{n+1}, VZ_i^{n+1})$ and (VX_i^n, VY_i^n, VZ_i^n) are the flow velocities on the nodes when $t = t^{n+1}$ and $t = t^n$, respectively. The travelling velocity of the particle during one sub-step is computed as

$$
VX = \frac{1}{2}(VX_Q + VX_P), \quad VY = \frac{1}{2}(VY_Q + VY_P), \quad VZ = \frac{1}{2}(VZ_Q + VZ_P) \tag{31}
$$

where (VX_P, VY_P, VZ_P) is the velocity of the source point *P*.

Substituting (28) into (27), the coordinate of the target point (X_Q, Y_Q, Z_Q) becomes functions of ξ and η. Substituting (30) into (29) and then the resultant equation into (31), one can see that the three components of the travelling velocity (VX, VY, VZ) are functions of θ, ξ, and η. Therefore, the location of the target point and the velocity at which the particle is travelling (and thus the elapsed travelling time) in the sub-step of backward particle tracking can be determined by three unknown parameters: θ, ξ, and η. The solution can be obtained by choosing any three out of the following four

equations to form a set of nonlinear equations, which can be solved with the Newton-Raphson method for the three unknowns.

$$X_Q - X_P = VX \cdot \Delta t^* \tag{32a}$$

$$Y_Q - Y_P = VY \cdot \Delta t^* \tag{32b}$$

$$Z_Q - Z_P = VZ \cdot \Delta t^* \tag{32c}$$

$$\sqrt{(X_Q - X_P)^2 + (Y_Q - Y_P)^2 + (Z_Q - Z_P)^2} = \sqrt{VX^2 + VY^2 + VZ^2} \cdot \Delta t^* \tag{32d}$$

where $\Delta t^* = t^{**} - (1-\theta) t^{n+1} - \theta t^n$, and t^{**} is the ending time of the previous sub-step. The example in Figure 4 shows the first sub-step in backward particle tracking, thus $t^{**} = t^{n+1}$ and $\Delta t^* = \theta(t^{n+1} - t^n) = \theta \Delta t$. Note that for each sub-step, the available tracking time equals $\Delta t - (t^{n+1} - t^{**})$. At the end of one sub-step (ending time $t = t^*$), if $t^* > t^n$, the target point is set as a new source point with $(X_P, Y_P, Z_P) = (X_Q, Y_Q, Z_Q)$ and $(VX_P, VY_P, VZ_P) = (VX_Q, VY_Q, VZ_Q)$, and the ending time of the previous sub-step is set to t^*. Thus a new sub-step of particle tracking starts. This procedure is repeated continuously until $t^* \le t^n$. If the particle reaches the boundary of the global element and available tracking time is not used up, then the neighbour global element is partitioned into sub-elements and the tracking continues. If the particle reaches the boundary of the computational domain, the tracking terminates.

3.4 Moving grid scheme

In the moving grid method, the mesh node fitted to the free surface must be repositioned each time the free surface is moved. In the ALE representation, the grid velocity of nodes can be specified arbitrarily, i.e. the movement of the node does not necessarily follow the local velocity of the fluid. In the proposed model, the water elevation of each free surface node is obtained explicitly by solving Equation (5) or (6).

The simplest version of mesh moving scheme is presented in this paper. As the free surface elevation changes, all the free surface nodes are moved in the *z*-direction to the new elevation to fit the free surface. Then other mesh nodes are repositioned uniformly along *z*-direction from the free surface to the river bed. This moving grid scheme requires that the moving contact boundaries must be vertical walls.

4. Preliminary verification

The classical sloshing problem with small deformation is used as a test case for preliminary model verification. Figure 5 shows a liquid column of width L and height H with a free surface. The initial surface profile shown in Figure 5 represents the first anti-symmetric mode of vibration, which is given by $\eta(x,0) = A\cos(\pi x / L)$, where A = 0.01 is the amplitude of the initial oscillation. The parameters used in the computation are as follows, H = 1, L = 1, ν=0.01, and g = 1.0. A no-slip condition is imposed on the bottom. The free-slip boundary condition is specified on the vertical walls. The computation was carried out on a 40 × 40 mesh with 1600 quadrilateral elements. Figure 6 shows the computed water surface elevation as a function of time at $x = 0$ and $x = L$. The result from the current work is in good agreement compared with the results from Ramaswamy (1990) and Braess et al. (2000).

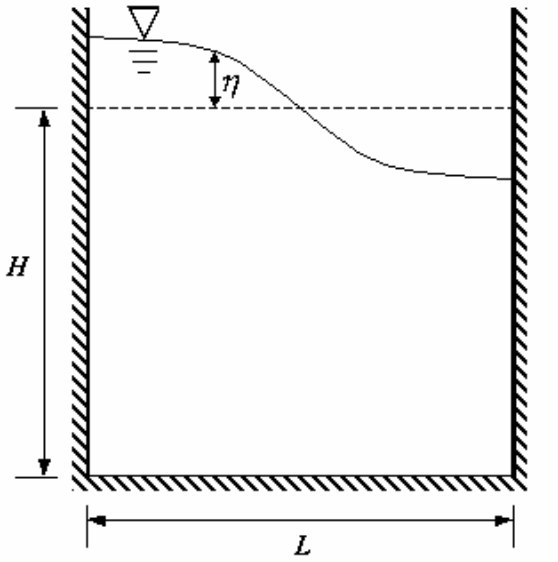

Figure 5 Schematic sketch of sloshing problem

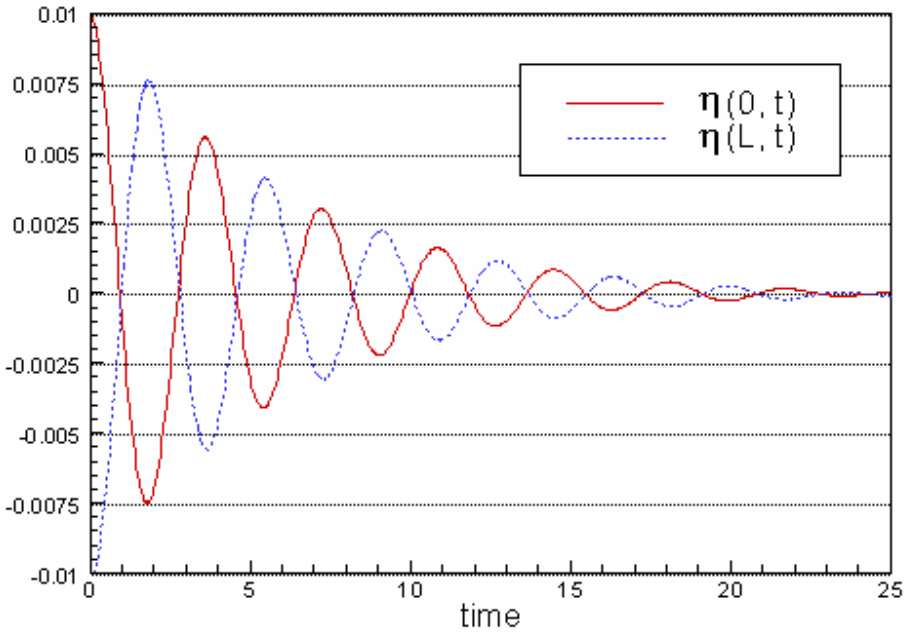

Figure 6 Computed history of free surface elevation

5. Model application to Loxahatchee River and Estuary

5.1 Study area and model setup

The study area is the watershed of the Loxahatchee River and Estuary located on the east coast of Florida within northern Palm Beach and southern Martin Counties. The Loxahatchee River connects to the Atlantic Ocean via the Jupiter Inlet near the city of Jupiter. The main water body consists of the estuary and several major tributaries of the river, including the North Fork, Southwest Fork, the Northwest Fork, and the North and South Intracostal Waterways. Figure 7 shows a map of the area and a top view of the model mesh. The model domain includes all the major tributaries of the river and a portion of the North and South Intracoastal Waterways. A part of the Atlantic Ocean to the east of Florida coastal line is also included in the model domain to incorporate the open-ocean boundary condition more appropriately.

The Loxahatchee River has often been referred to as the “last free flowing river in southeast Florida”. The Northwest Fork of the river also represents one of the largest vestiges of native cypress river-swamp within southeast Florida. During the past century, the natural hydrologic regime of this area has been altered dramatically due to agricultural and residential development. The construction of canals for drainage and flood protection has diverted much of the surface flow to the Southwest Fork of the river. Now the flow in the river and estuary is under the influence of tide from the Atlantic Ocean. Periodic saltwater intrusion has threatened the freshwater cypress trees and many other species in the area. The goal of present work is to apply the bay/estuary model to simulate hydrodynamics and salinity transport in the Loxahatchee River.

The mesh shown in Figure 7 is used as the base to generate the three-dimensional finite element mesh, which has of four elements in the vertical direction extended from the river bed to the water surface, and the grid nodes are uniformly distributed in the vertical direction, as shown in Figure 8. The surface water domain is partitioned into 5,224 hexahedral or triangular prism elements with 32,064 quadratic nodes or 9,105 linear nodes. In the horizontal direction, the size of the elements is about 3,500 ft in the Atlantic Ocean and about 15 ft near the Kitching Creek. The bathymetry in the domain ranges from -22 ft to -1 ft (NGVD29). The size of elements varies between 6 ft and 0.6 ft in the vertical direction. The South Florida Water Management District (SFWMD) has collected water elevation and salinity data with a frequency of 15 minutes at the following stations in the model domain: Coastal Guard Dock (CGD), Pompano Drive (PD), Boy Scout Dock (BSD), Kitching Creek (KC), and River Mile 9 (RM9), as marked in Figure 7 and Figure 8.

In the Loxahatchee River area, tide is the major driving force of the surface water system in model domain. Because no tidal data is available at the open-ocean boundary of the model, we extrapolated the water elevation data at CGD to the ocean boundary with a 15-minute time shift. The fresh water inflow at the upstream of the tributaries of the river is obtained from field data. A constant salinity of 35.5 parts per thousand (ppt) is set at the open-ocean boundary. Precipitation and evaporation are not considered in the

current model run. A simulation was conducted for a time period from 12/1/2003 – 12/31/2003.

Figure 7 A map of the Loxahatchee River and Estuary and model mesh.

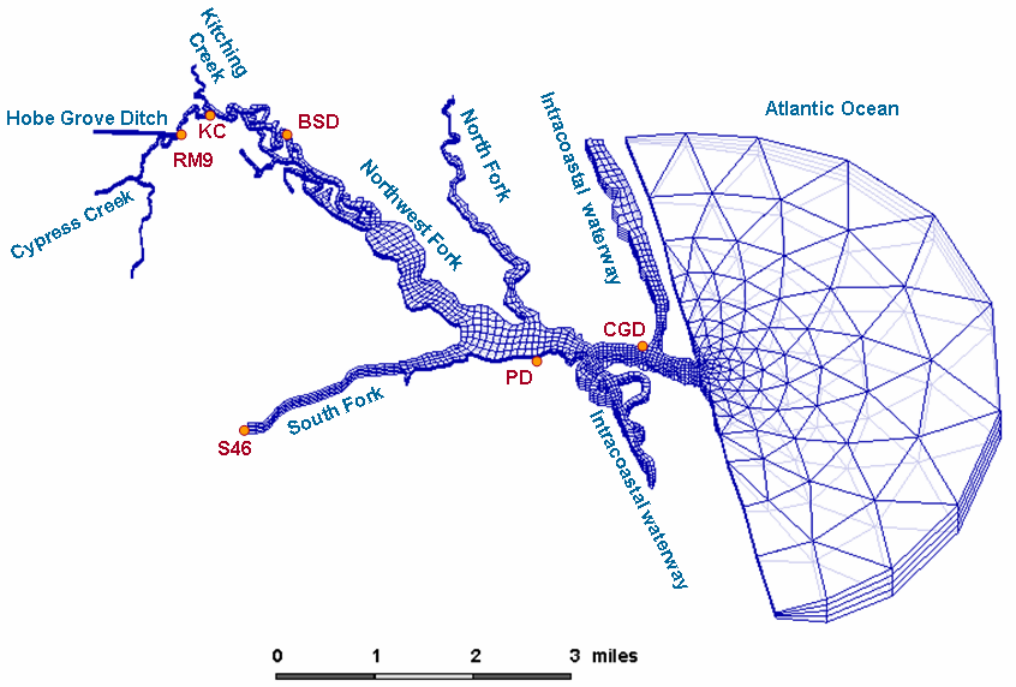

Figure 8 Three-dimensional model mesh.

5.2 Simulation results

The model output includes water surface elevation, water depth, flow velocity, and salinity field. Figure 9 shows the distribution of salinity in the river at t = 400 hour. The time history of water stage and salinity predicted by the model are compared with the field data collected at surface water stations along the river. Figure 10 through Figure 14 display the model output (M) water stage in comparison with the field data (F) at CGD, PD, BSD, KC, and RM9 stations. The model output matches well with the field data.

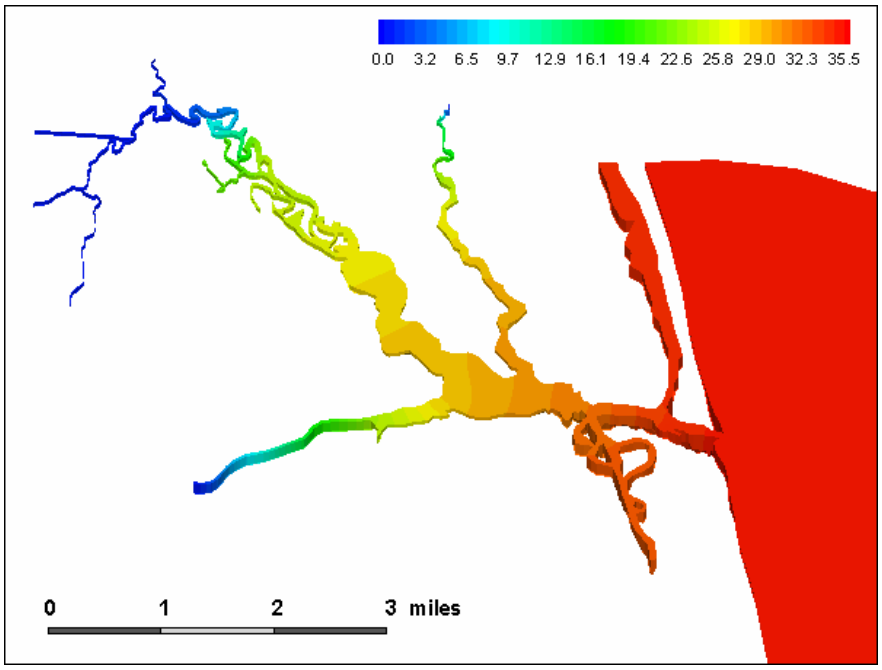

Figure 9 Distribution of salinity (ppt) in the river at t = 400 hour.

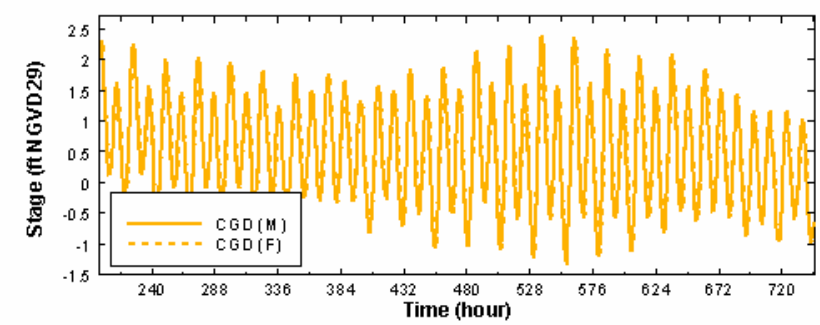

Figure 10 Model output water stage at Coastal Guard Dock (CGD) in comparison with field data

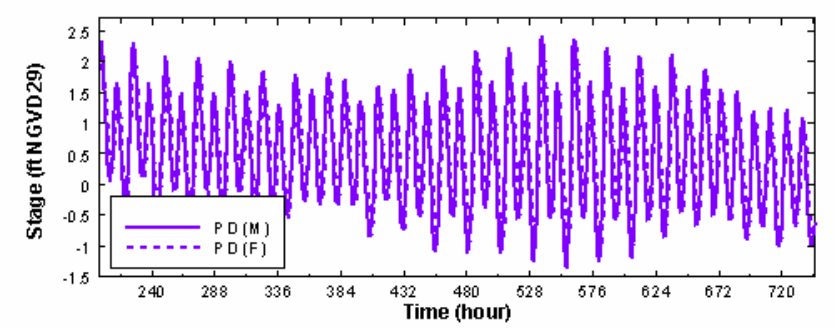

Figure 11 Model output water stage at Pompano Drive (PD) in comparison with field data

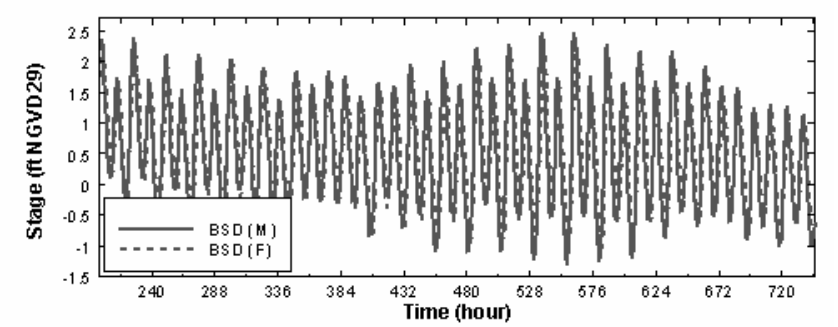

Figure 12 Model output water stage at Boy Scout Dock (BSD) in comparison with field data

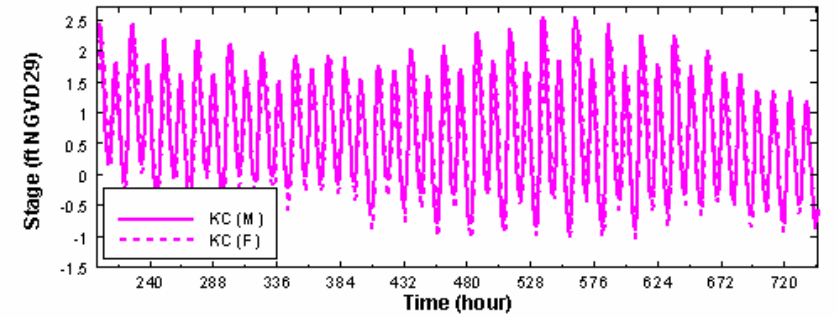

Figure 13 Model output water stage at Kitching Creek (KC) in comparison with field data

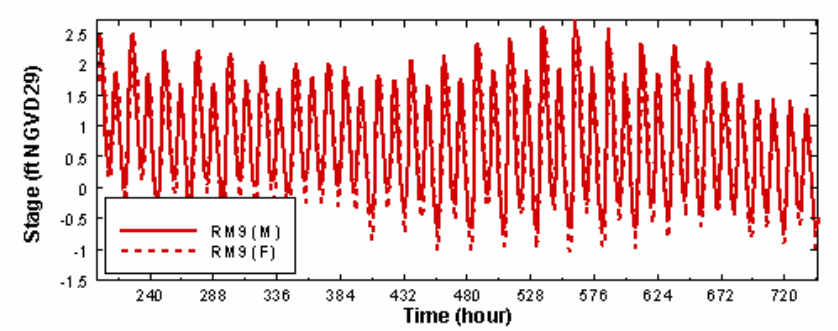

Figure 14 Model output water stage at River Mile 9 (RM9) in comparison with field data

The comparisons between the model output (M) salinity level and field data (F) at CGD, PD, BSD, KC, and RM9 stations are shown in Figure 15 through Figure 19. Overall, the model output salinity agrees reasonably well with field data at all stations.

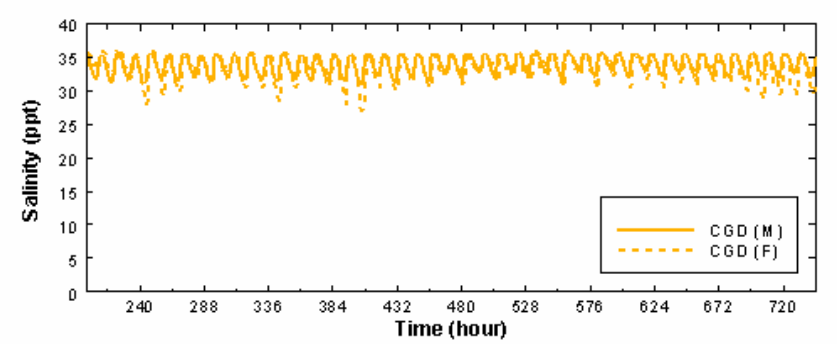

Figure 15 Model output salinity at Coastal Guard Dock (CGD) in comparison with field data

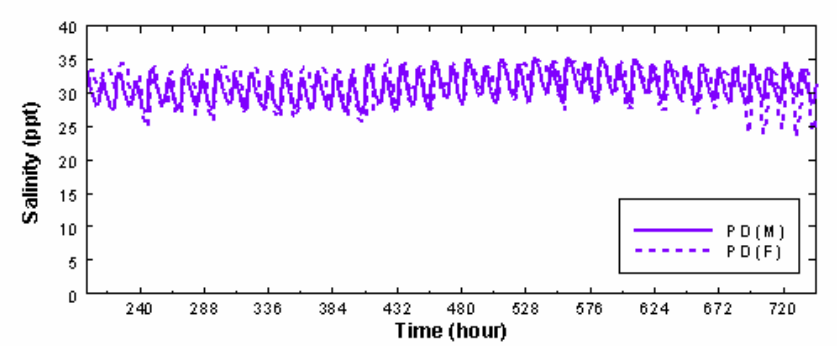

Figure 16 Model output salinity at Pompano Drive (PD) in comparison with field data

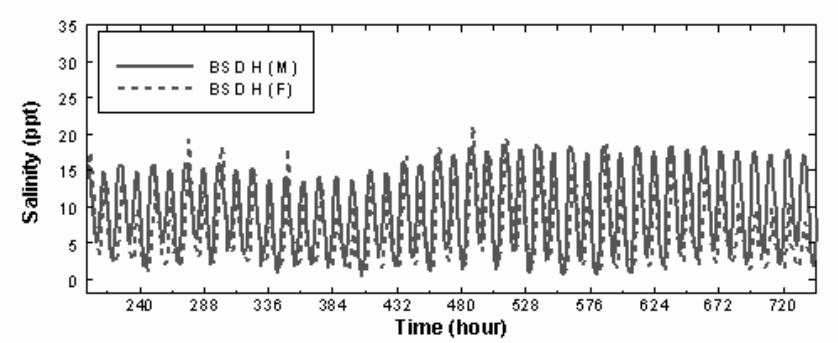

Figure 17 Model output salinity at Boy Scout Dock (BSD) in comparison with field data

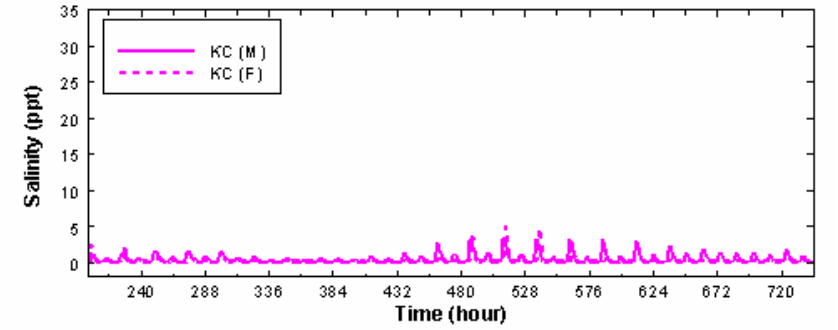

Figure 18 Model output salinity at Kitching Creek (KC) in comparison with field data

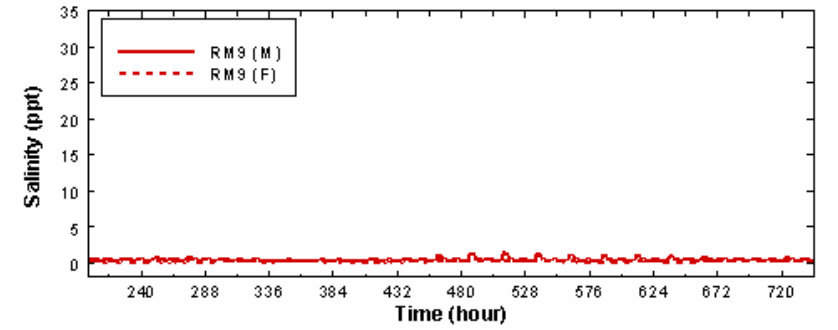

Figure 19 Model output salinity at River Mile 9 (RM9) in comparison with field data

The root mean squared error (*rms*), the Pearson product-moment correlation coefficient (R^2), and the Theil's inequality coefficient (U^2) are used to quantitatively assess the model performance in simulating the surface water flow and salinity transport. The *rms* error is defined by

$$\varepsilon_{rms} = \sqrt{\frac{1}{N}\sum_{i=1}^{N}\left(\Phi_F(t_i) - \Phi_M(t_i)\right)^2} \tag{33}$$

where N is the total number of samples, $\Phi_F(t_i)$ is the value of field measurement at $t = t_i$, $\Phi_M(t_i)$ is the value of model prediction at $t = t_i$. Because the *rms* error measure gives greater weight to larger discrepancy than smaller ones, it is more sensitive than other measures to the occasional large error and thus is considered as the most rigorous absolute error test.

The Pearson product-moment correlation coefficient is defined by

$$R^2 = \left(\frac{\sum_{i=1}^{N}\left(\Phi_F(t_i) - \overline{\Phi}_F\right)\left(\Phi_M(t_i) - \overline{\Phi}_M\right)}{\sqrt{\sum_{i=1}^{N}\left(\Phi_F(t_i) - \overline{\Phi}_F\right)^2 \sum_{i=1}^{N}\left(\Phi_M(t_i) - \overline{\Phi}_M\right)^2}} \right)^2 \tag{34}$$

where $\overline{\Phi}_F = \frac{1}{N}\sum_{i=1}^{N}\Phi_F(t_i)$, and $\overline{\Phi}_M = \frac{1}{N}\sum_{i=1}^{N}\Phi_M(t_i)$. R^2 measures the degree of linear association between the field observation and model prediction. It represents the amount of variability of one variable that is explained by correlating it with another variable. R^2 varies from 0 to 1 with 1 indicating a perfect fit.

Theil's inequality coefficient is defined by

$$U^2 = \frac{\sum_{i=1}^{N}\left(\Phi_F(t_i) - \Phi_M(t_i)\right)^2}{\sum_{i=1}^{N}\left(\Phi_M(t_i)\right)^2} \tag{35}$$

U^2 was originally designed to evaluate econometric model forecasts and can be applied to environmental and ecological models as well. $U^2 = 0$ means that the model is perfect in its prediction, and $U^2 = 1$ means that the model is not reliable.

The root mean squared error, the correlation coefficient, and the Theil's coefficient for both water stage and salinity at the three field stations are given in Table 1. In this comparison, the frequency of field data is 15 minutes. Overall, satisfactory results are

obtained in modeling the water stage. Since the predication of salinity transport is usually more difficult, the results in modeling salinity are not as satisfactory.

Table 1. Statistical test of model prediction error

Location	Water Stage			Salinity		
	rms **(ft)**	R^2	U^2	***rms*** **(ppt)**	R^2	U^2
Coastal Guard Dock (CGD)	0.0787	0.9936	0.00624	1.15	0.5803	0.001136
Pompano Drive (PD)	0.328	0.8653	0.105	2.09	0.6362	0.004530
Boy Scout Dock (BSD)	0.316	0.8758	0.0920	4.39	0.6700	0.1192
Kitching Creek (KC)	0.260	0.9099	0.0577	0.849	0.2423	0.6268
River Miles 9 (RM9)	0.254	0.9156	0.0517	0.208	0.5650	0.3094

The above quantitative statistics indicate that the variations in tides are well explained at all five stations and the predictabilities of tides are excellent at all five stations. The variations in salinity are fairly explained at all five stations except for KC. The R^2 for KC and RM9 are statistically less meaningful because the field data at these two stations are almost constant. The predictability in salinity is excellent at CGD and PD, fair at BSD and RM9, and poor at KC. It is surmised that the groundwater may have more influence in salinity at the inland stations (BSD, RM9, and KC) than at the coastal stations (CGD and PD). Further investigations in the poor performance of predictions at inland stands, in particular at KC, need to be conducted.

6. Conclusions

We have developed a three-dimensional hydrodynamics and transport model for bay/estuary based on Navier-Stokes equations in ALE form combined with the moving grid approach. The numerical solution is obtained using finite element method or a mixed Lagrangian-Eulerian (particle tracking) and finite element method. The model has been successfully calibrated against field tidal, but not as satisfactory in salinity data. After further improvement in calibrating salinity data, the model can be applied to Loxahatchee Estuary for the investigation of its minimum flow requirements to maintain ecological balance. The future work may include the development an integrated surface and groundwater model for the study area to improve model performance in salinity data at inland stations.

Acknowledgments

This work was supported in part by South Florida Water Management District and Florida Department of Environmental Protection. G. T. Yeh is supported in part by National Center for High Performance Computing (NCHC) in Taiwan while he takes a one-year sabbatical leave therein.

References

Benque, J.P., Cunge, J.A., Feuillet, J., Hauguel, A., Holly, F.M., 1982. New method for tidal current computation. *ASCE Journal of Waterways, Port, Coastal and Ocean Division* 108, 396-417

Braess, H., P. Wriggers, 2000. Arbitrary Lagrangian Eulerian finite element analysis of free surface flow. *Computational Methods in Applied Mechanical Engineering* 190, 95-109

Brooks, A.N., Hughes, T.J.R., 1982. Streamline upwind Petrov-Galerkin formulation for convection dominated flows with particular emphasis on the incompressible Navier-Stokes equations. *Computer Methods in Applied Mechanics and Engineering* 32, 199-259.

Chan, R.K.C., 1975. A general arbitrary Langrangian-Eulerian method for incompressible flows with sharp interfaces. *Journal of Computational Physics* 17, 311-331.

Cheng, H. P., Cheng, J. R., and Yeh, G. T., 1996. A particle tracking technique for the Lagrangian-Eulerian finite element method in multi-dimensions. *International J. Numerical Methods in Engineering*, 39(7), 1115-1136.

Drago, M., Iovenitti, L. 2000. σ-Coordinates hydrodynamic numerical model for coastal and ocean three-dimensional circulation. *Ocean Engineering* 27, 1065-1085.

Duwe, K.C., Hewer, R.R., Backhaus, J.O., 1983. Results of a semi-implicit two-step method for the simulation of markedly nonlinear flow in coastal seas. *Continental Shelf Research* 2, 255-273.

Güler, I., Behr, M., Tezduyar, T. 1999. Parallel finite element computation of free-surface flows. *Computational Mechanics* 23, 117-123.

Harlow, F.H., Welch, J.E., 1965. Numerical calculation of time dependent viscous incompressible flow with free surface. *Physics of Fluids* 8, 2182-2189.

Hirt, C.W., Nichols, B.D., 1981. Volume of fluid (VOF) method for dynamics of free boundaries. *Journal of Computational Physics* 39, 201-221.

Kim, C., Lee, J., 1994. A three-dimensional PC-based hydrodynamic model using an ADI scheme. *Coastal Engineering* 23, 271-287.

Le Provost, Genco, C., Lyard, F., 1995. Modeling and predicting tides over the world ocean, quantitative skill assessment for coastal ocean models. *Coastal and Estuarine Studies* 47, 175-201.

Ramaswamy, B., 1990. Numerical simulation of unsteady viscous free surface flow. *Journal of Computational Physics* 90, 396-430.

Sauvaget, P., David, E., Guedes Soares, C., 2000. Modelling tidal currents on the coast of Portugal. *Costal Engineering* 40. 393-409.

Shan, H., Yeh, G.T., 2004. A three-dimensional finite element model for free surface flows. *Computational Fluid Dynamics Journal* 13, 552-560.

Shankar, N.J., Cheong, H.F., Sankaranarayanan, S., 1997. Multilevel finite-difference model for three-dimensional hydrodynamic circulation. *Ocean Engineering* 24, 785-816.

Umlauf, L, Burchard, H., 2003. A generic length-scale equation for geophysical turbulence models. *J. Marine Res.* 61, 235-265.

Warner, J.C., Shervwood, C.R., Arango, H.G., Signell, R.P., 2005. Performance of four turbulence closure models implemented using a generic length scale method. *Ocean Modelling* 8, 81-113.

Zhang, Q.Y., Gin, K.Y.H., 2000. Three-dimensional numerical simulation for tidal motion in Singapore's coastal waters. *Coastal Engineering* 39, 71-92.